# Tube-wave reflections in cased borehole

Alexandrov D.V.
Saint-Petersburg State University
Department of Physics
Laboratory of Elastic Media Dynamic

April 13, 2008

## Summary

At low frequencies tube or Stoneley waves represent a dominant arrival propagating along boreholes. They can be excited by the source in a well or by external source due to conversion from other wave types. Tube wave experiences reflection at the bed boundaries, borehole diameter changes and fractures or permeable zones. It was proven in previous studies that 1D effective wavenumber approach provides simple and accurate low-frequency description of tube-wave propagation in open boreholes surrounded by radially homogeneous formation. Tube waves become even more dominant in cased boreholes, but casing further modifies wave propagation and reflection/transmission phenomena. In this study we apply 1D effective wavenumber approach to radially inhomogeneous media and demonstrate that it still provides excellent description of low-frequency tube-wave propagation. In particular, we focus on three models representative of cased boreholes: reflection from geological interfaces behind casing, reflection from corroded casing section and reflection from idealized disk-shaped perforation in cased hole. In all three cases frequency-dependent reflection coefficient obtained by 1D effective method and by finite-difference computations show excellent agreement.

## 1 Introduction

Tube (Stoneley) waves are useful for characterizing near-wellbore space since they are sensitive to borehole diameter changes, variations in elastic properties and permeability of the surrounding formations. The main part of tube-wave energy is concentrated inside the well. In open-hole acoustic logging higher-frequency tube waves are used to detect and characterize fractures as well as to obtain a permeability profile (Winkler et al., 1989; Krauklis and Krauklis, 2005). In cased boreholes low-frequency tube-wave reflections can be used for estimation of quality and parameters of hydraulic fractures (Medlin and Schmitt, 1994; Paige et el., 1995) as well as other purposes. We are interested in the latter applications for cased boreholes where surrounding media is radially inhomogeneous (casing, cement, formation). Currently only numerical finite-difference methods can handle the reflection/transmission problem for such systems. Finite-difference method provides little physical insight into the problem. Approximate methods are useful for gaining better understanding of the problem of tube-wave reflections in cased boreholes. In this study we utilize 1D effective wavenumber approach suggested by White (1983) and extended by Tang and Cheng (1993). This approach was originally developed for low-frequency tube waves in radially homogeneous formations and was verified numerically for an open hole surrounded by elastic (Tezuka et al, 1997) and poroelastic formations (Bakulin et al., 2005). Here we extend this approach to radially inhomogeneous media with particular focus to cased boreholes.

## 2 1D effective wavenumber approach

The problem of acoustic logging can be considered either from the point of exact analytical solution or using numerical modelling. Good understanding of physical processes can be obtained from analytical solutionis, however the main disadvantage is the fact that amount of models which can be solved analytically is rather limited. Such models are the simplest like borehole in homogenous isotropic or anisotropic media. Therefor, more complex models, like fluid-filled wells with varying diameter, or cased boreholes, are usually solved with numerical methods or approximate analytical methods. The last ones need to be examined for adaptability and one of the simplest and most effective is to compare results of approximate analytical methods with correspondent numerical modelling.

Approximate analytical method I have used in this work is 1D effective wavenumber approach. Original formulation of 1D approach by White (1983) and later generalization by Tang and Cheng (1993) assumed radial homogeneity of the media surrounding the fluid column. This was appropriate to describe open-hole acoustic logging. While change in diameter (washout) could be treated, no radial layering was assumed beyond the fluid-formation interface. Our interest lies in analyzing interaction of tube waves with borehole structures in cased wells. Casing (and cement) represents another radial layer with very distinct parameters that substantially alters the properties of the tube wave (velocity, dispersion, attenuation) and ultimately modifies the reflection and transmission phenomena in an unknown manner. It seems that only numerical methods, like finite-difference, can correctly handle these interactions. Nevertheless, presence of elastic or poroelastic radial layering without additional fluid layers still supports only one propagating tube wave albeit with modified properties. Thus, it appears reasonable to assume that at least at low frequencies extension of 1D approach should still be applicable. Let us verify this hypothesis by means of a series of numerical tests.

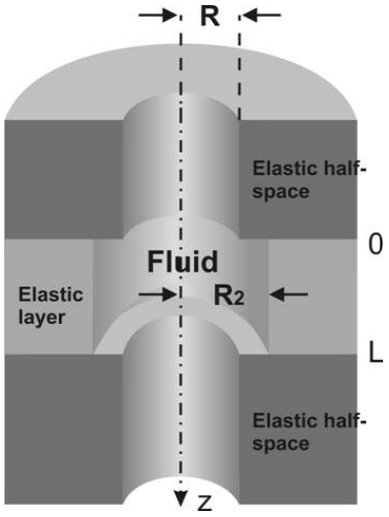


Fig. 1: Fluid-filled borehole penetrates elastic layer embedded between two elastic half-spaces

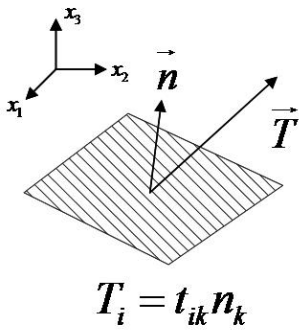


Fig. 2: Stress vector **T** is applied to a small area with normal vector **n**

First, let us review the basics of 1D effective wavenumber approach (Tang and Cheng, 1993; Bakulin et al, 2005). Consider a layer embedded between two equal half-spaces (figure 1). Coordinates of upper and lower layer boundaries are $z = 0$ and $z = L$. Borehole intersect this layer and has radius $R_1$ outside the layer and $R_2$ inside. Tube-wave propagation is described with Helmholtz

equation (2.1) where $\phi(z)$ is tube-wave potential, $k_1$ is Stoneley wavenumber outside the layer, $k_2$ - inside. Pressure and displacements can be found according to the equalities (2.2). Here $\rho_f$ is fluid density and $\omega$ - cyclic frequency.

$$\begin{aligned} \frac{\partial^2\phi_1(z)}{\partial z^2} + k_1\phi_1(z) = 0 \quad z < 0,\ z > L \\ \frac{\partial^2\phi_2(z)}{\partial z^2} + k_2\phi_2(z) = 0 \quad 0 < z < L \end{aligned} \tag{2.1}$$

$$P = \rho_f\omega^2\phi, \quad U = \frac{\partial\phi(z)}{\partial z} \tag{2.2}$$

Solution of equation can be found in the following form:

$$\begin{aligned} \phi_1 = e^{ik_1z} + R_1e^{-ik_1z}, \\ \phi_2 = T_2e^{ik_2z} + R_2e^{-ik_2z}, \quad \phi_3 = T_3e^{ik_3z} \end{aligned} \tag{2.3}$$

,

where $R$ and $T$ are designations for reflection and transmission coefficients. To obtain these coefficients mass balance boundary conditions are set at each interface, in particular continuity of pressure and fluid flow (2.4).

$$\begin{aligned} &\text{Continuity of pressure:} \quad P_1(0) = P_2(0), \quad P_2(L) = P_3(L) \\ &\text{Continuity of fluid flow:} \quad \oint\limits_S \overrightarrow{V}\overrightarrow{N}dS = 0 \end{aligned} \tag{2.4}$$

This results in a system of linear equation, and solutions of this system are reflection and transmission coefficients from a layer embedded between two equal half-spaces (2.5).

$$\begin{aligned} R = \frac{2i(k_2^2s_2^2 - k_1^2s_1^2)\sin k_2L}{(k_2s_2 + k_1s_1)^2e^{-ik_2L} - (k_2s_2 - k_1s_1)^2e^{ik_2L}} \\ T = \frac{4k_2k_1s_2s_1e^{-ik_2L}}{(k_2s_2 + k_1s_1)^2e^{-ik_2L} - (k_2s_2 - k_1s_1)^2e^{ik_2L}} \end{aligned} \tag{2.5}$$

Here $s$ is cross section area.

Now consider a multilayered model. The system of parallel-sided layers is intersected with fluid-filled well with different radius in each layer. Like previous case in each vertically homogeneous zone tube-wave propagation is described with 1D differential equations.

$$\frac{\partial^2\phi_i(z)}{\partial z^2} + k_i\phi_i(z) = 0 \tag{2.6}$$

Therefore wave potentials can be found in the following form:

$$\phi_i = A_ie^{ik_iz} + B_ie^{-ik_iz}, \tag{2.7}$$

where $k_i$ is wavenumber, $A_i$ and $B_i$ - amplitude coefficients of up-going and down-going waves. It is clear that interference reflection and transmission coefficients can be obtained from the equalities (2.8).

$$R = \frac{B_1}{A_1}, \quad T = \frac{A_N}{A_1} \tag{2.8}$$

Boundary conditions are the same as in the previous case, and we obtain a system of linear equations where G is a propagation matrix (2.10).

$$\begin{aligned} &\text{Continuity of pressure:} \quad P_{i-1}(z_i) = P_i(z_i) \\ &\text{Continuity of fluid flow:} \quad \oint\limits_{S_i} \overrightarrow{V}\overrightarrow{N}dS = 0 \end{aligned} \tag{2.9}$$

$$\begin{gathered} \begin{pmatrix} B_i \\ A_i \end{pmatrix} = G_i \begin{pmatrix} B_{i+1} \\ A_{i+1} \end{pmatrix} \\ \begin{pmatrix} B_1 \\ A_1 \end{pmatrix} = G_1 \begin{pmatrix} B_2 \\ A_2 \end{pmatrix} = ... = G_1 G_2 ... G_{N-1} \begin{pmatrix} B_N \\ A_N \end{pmatrix} := G_T \begin{pmatrix} B_N \\ A_N \end{pmatrix} \end{gathered} \tag{2.10}$$

$$R = \frac{(G_T)_{12}}{(G_T)_{22}}, \quad T = \frac{1}{(G_T)_{22}} \tag{2.11}$$

Although equations (2.5) and (2.11) are obtained for homogeneous formation, we may apply them without modification for radially inhomogeneous formation, provided that Stoneley wavenumber is now computed for multi-layered model at hand. For simplicity in this study we assume radially layered model with three layers: fluid, casing and formation. In this case effective wavenumber $k$ as a function of frequency is calculated numerically from set of equations representing boundary conditions and assuming full bond between casing and formation. Once effective wavenumbers are established for each vertically homogeneous zone, equations (2.11) are used to compute the reflection coefficient as a function of frequency and compare them with the corresponding quantities found from finite difference modeling. Small tube-wave dispersion in cased boreholes allowed us to use frequency-independent velocities in all numerical examples below since computations with and without frequency dependence of the wavenumber are almost identical. Material parameters for all models are summarized in Table 1.

# 3 Wavefield in cased borehole

## 3.1 Wavefield in isotropic homogeneous fluid

The key question now is how to obtain the wavenumber. Let's consider homogeneous isotropic fluid. Oscillations of fluid are described with equation (3.1.1), which is a form of Newton's second low. Here $\rho_f$ is fluid density, $u$ - fluid displacement and $t_{ik}$ - stress tensor.

$$\rho_f \frac{\partial^2 u_i}{\partial t^2} = \frac{\partial t_{ik}}{\partial x_k}, \quad t_{ik} = \lambda_f \delta_{ik} \text{div}\,\overrightarrow{u} = -p\delta_{ik} \tag{3.1.1}$$

To understand stress tensor sense consider a small area with a normal vector $\overrightarrow{n}$ and a stress vector $\overrightarrow{T}$ applied to this area (figure 2). Then components of this vector can be easily recovered provided stress tensor components are known. If we substitute this expression in first equation, we will obtain following equality:

$$\rho_f \frac{\partial^2 u_i}{\partial t^2} = \lambda_f \text{grad div}\,\overrightarrow{u}. \tag{3.1.2}$$

Here homogeneity of the media was used, that is independence of elastic constant $\lambda_f$ from spatial coordinates. It is convenient to solve this equation in terms of fluid pressure. If we consider system

with point source, than we should put delta-function in the right side of the equation.

$$\Delta p(x,y,z,t) - \frac{1}{v_f^2} p(x,y,z,t) = \delta(t)\delta(x,y,z), \quad p = -\text{div}\,\overrightarrow{u}, \quad \frac{1}{v_f^2} = \frac{\lambda_f}{\rho_f} \tag{3.1.3}$$

$$\Delta P(r,k,\omega) - \frac{\omega^2}{v_f^2} P(r,k,\omega) = \delta(r) \tag{3.1.4}$$

Time and Spatial Fourier transform leads to the equation (3.1.4). For the system has axial symmetry, one can rewrite this equation in cylindrical coordinates and obtain so-called Bessel equation of zero-order. Solution of this equation are Bessel- and Hankel-function of zero-order. Solutions for pressure and for displacement are presented below.

$$P(r,k,\omega) = C_f J_0(-i\alpha_f r) + \frac{i}{4} H_0^{(2)}(-i\alpha_f r), \quad \alpha_f = \omega\sqrt{\frac{k^2}{\omega^2} - \frac{1}{v_f^2}}, \quad r = \sqrt{x^2+y^2} \tag{3.1.5}$$

$$\begin{pmatrix} U_r \\ U_z \end{pmatrix} = C_f \begin{pmatrix} \alpha_f J_1(-i\alpha_f r) \\ -k J_0(-i\alpha_f r) \end{pmatrix} - \frac{1}{4\rho_f\omega^2} \begin{pmatrix} \alpha_f H_1^{(2)}(-i\alpha_f r) \\ -k H_0^{(2)}(-i\alpha_f r) \end{pmatrix} \tag{3.1.6}$$

One can see that for infinite fluid with point source we have one unknown constant $C_f$ (independent from spatial coordinates). Here $k$ is wavenumber.

## 3.2 Wavefield in isotropic homogeneous elastic media

Now consider infinite homogeneous elastic media.

$$\rho_f \frac{\partial^2 u_i}{\partial t^2} = \frac{\partial t_{ik}}{\partial x_k}, \quad t_{ik} = \lambda_f \delta_{ik} \text{div}\,\overrightarrow{u} + 2\mu\epsilon_{ik} \tag{3.2.1}$$

For such media additional component appears in stress tensor (3.2.1). It contains strain tensor $\epsilon_{ik}$, which for small deformations has following form:

$$\epsilon_{ik} = \frac{1}{2}\Big(\frac{\partial u_i}{\partial x_k} + \frac{\partial u_k}{\partial x_i}\Big) \tag{3.2.2}$$

$$\rho_f \frac{\partial^2 u_i}{\partial t^2} = (\lambda + 2\mu)\text{grad div}\,\overrightarrow{u} - \text{rot rot}\,\overrightarrow{u} \tag{3.2.3}$$

In this case motion equation becomes more complicated (3.2.3), but it still can be solved. After time- and spatial fourier transform we will again obtain Bessel equation. But now there will be two kinds of waves: p-wave (from primal) and s-wave (from secondary).

$$\begin{pmatrix} U_r \\ U_z \end{pmatrix} = C_p \begin{pmatrix} \alpha_p H_1^{(2)}(-i\alpha_p r) \\ -k H_0^{(2)}(-i\alpha_p r) \end{pmatrix} + C_s \begin{pmatrix} \alpha_s H_1^{(2)}(-i\alpha_s r) \\ -k H_0^{(2)}(-i\alpha_s r) \end{pmatrix} \tag{3.2.4}$$

## 3.3 Boundary conditions

Now we should construct solution for the model we are interested in: cased borehole in homogeneous media (figure 3).

Casing, a steel pipe, has thickness $a$ and inner radius $R$. Solutions in previous sections were obtained for infinite media and thus contain only outgoing waves. It's clear that inside the casing wavefield will be described with expression from the previous (3.2.4), but there will be also waves

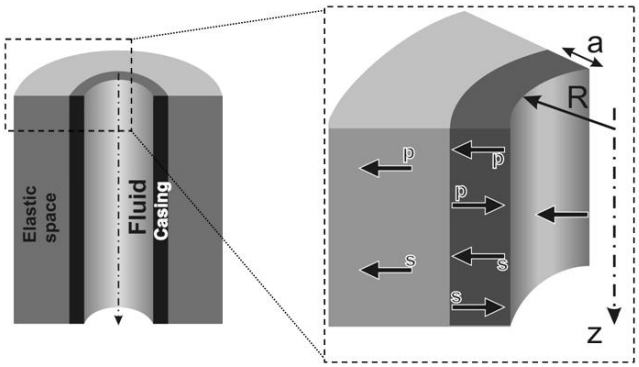


Fig. 3: Cased borehole in homogeneous elastic media

going in negative r-direction. Thus we have seven unknown constants: one in fluid, four in casing and two in surrounding elastic media. To obtain them we should set boundary conditions at each interface. They are:

- continuity of r-component of displacement on the boundary between fluid and casing:
  $U_r(R+0) = U_r(R-0)$,
- continuity of displacement on the boundary between casing and surrounding media:
  $\overrightarrow{U}(R+a+0) = \overrightarrow{U}(R+a-0)$,
- continuity of stress-vector components:
  $t_{rr}|_{R+0} = t_{rr}|_{R-0}, \quad t_{rr}|_{R+a+0} = t_{rr}|_{R+a-0},$
  $t_{rz}|_{R+0} = t_{rz}|_{R-0}, \quad t_{rz}|_{R+a+0} = t_{rz}|_{R+a-0}.$

There is no necessity in continuity of z-component of displacement because oscillation of fluid and casing in z-direction are independent - fluid is nonviscous and therefore there is no friction on the boundary between fluid and casing.

So, we have seven constants to find and a system of seven linear algebraic equations. After we inverse matrix of this system we can obtain them as functions of frequency, wavenumber and media elastic parameters.

$$M\overrightarrow{C} = \overrightarrow{D} \quad \Longrightarrow \quad \overrightarrow{C} = \frac{\widehat{M}}{\det M}\overrightarrow{D}$$
$$\overrightarrow{C} = \{C_f, C^c_{p+}, C^c_{p-}, C^c_{s+}, C^c_{s-}, C^e_{p+}, C^e_{p-}\} \tag{3.3.1}$$

But if determinant of this matrix is equal to zero for some values of parameters, then a singularity will appear. This condition (det M = 0) leads to an equation, called ”dispersion equation”. From dispersion equation one can obtain wavenumber as function of frequency for several wave modes. The slowest one is tube wave.

# 4 Modelling results

## 4.1 Reflection from geological interfaces behind casing

Figure 4 depicts the first model where cased borehole penetrates two thin horizontal layers. At low frequencies these two layers generate a composite tube-wave reflection that can be computed using equations similar to 2.5 but generalized to a four-layered 1D model. Figure 5 shows a comparison of reflection coefficients obtained with 1D approachand a finite-difference code jointly developed by Keldysh Institute of Applied Mathematics and Shell. In the latter case reflection coefficients are estimated by taking spectral ratios of reflected and incident tube waveforms. Good agreement between the two sets of curves proves that the effective wavenumber approach does capture the most important features of tube-wave interactions with formations in cased boreholes. When softer (plastic) casing is used the tube-wave reflections are larger indicating increased sensitivity to variations of elastic parameters behind the casing as it is intuitively expected, while in case of steel casing this sensitivity is muted due to stronger containment of the tube wave.

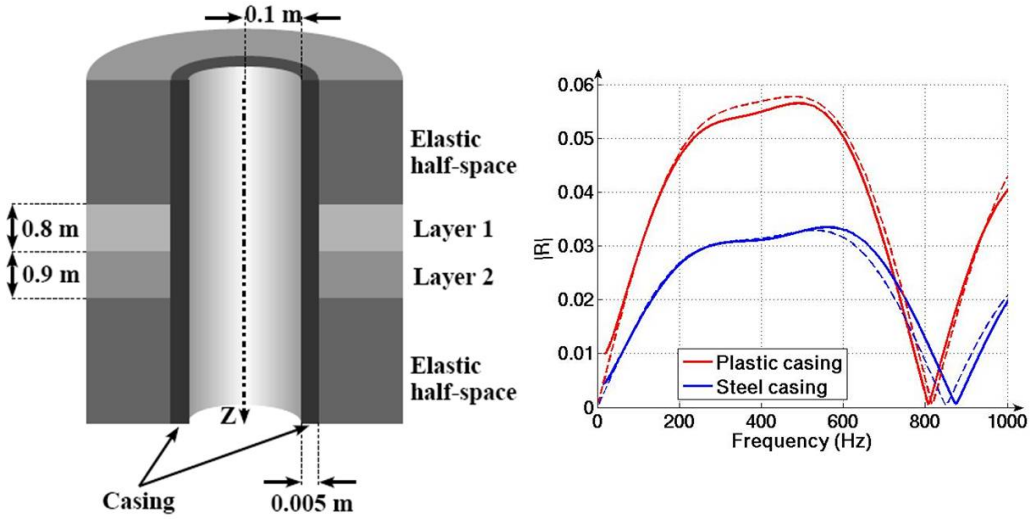


Fig. 4: Cased borehole intersects two elastic layers embedded between two elastic half-spaces.

Fig. 5: Reflection of the tube wave in Model 1 for two cases: plastic casing (red line) and steel casing (blue line). Solid lines indicate coefficients obtained numerically with finite-difference code, while dashed lines represent results of 1D effective wavenumber approach.

## 4.2 Reflection from corroded section of the casing

This section tests the 1D effective wavenumber approach for the case when variation in elastic parameters occurs in the properties of the first elastic layer - casing. The system under consideration is cased borehole surrounded by homogeneous formation (Figure 6). Casing has a corroded section with 0.8 m height. Density, longitudinal and shear velocities of corroded section are all reduced by the same multiplier Q (0.2, 0.5 and 0.7) compared to the properties of non-corroded section. Material parameters are given in the table below. Figure 7 confirms excellent agreement between approximate reflection coefficients obtained with 1D approach and ground truth response computed with

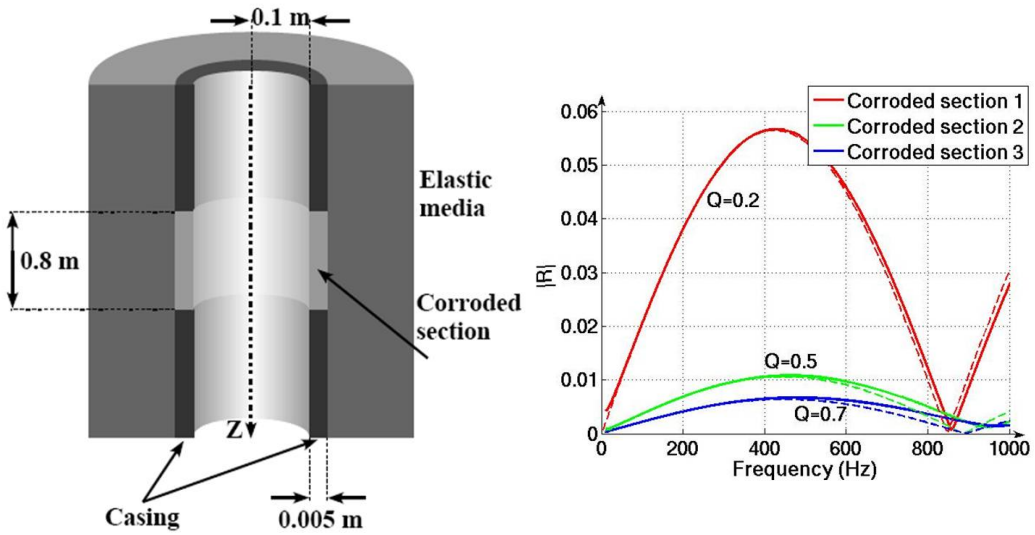


Fig. 6: Cased borehole in homogeneous elastic media; middle section of casing with 0.8 m height is corroded.

Fig. 7: Reflection of tube wave from three different types of corroded section: the highest reflection corresponds to the maximum difference between parameters of casing and corroded region.

finite-difference modeling. Notice that for reflection coefficient to become larger than 1%, elastic parameters of corroded region need to be reduced by at least factor of two.

## 4.3 Idealized perforation in cased borehole

Given success in describing tube-wave interaction for cased borehole with constant radius, we decided to explore more complicated models with varying borehole diameter. In particular, we focus on ”idealized perforation model” (Bakulin et al., 2005) depicted on Figure 8. While the material parameters in this model are identical to those for the corroded casing model of Figure 6 (except for corroded section), the key distinction is that instead of corroded region there is now disk-shaped perforation. Since formation is modeled as impermeable elastic space then effects related to fluid mobility between borehole and formation are neglected and only reflection due to geometric (diameter) changes are considered. Real perforation represents a small cylinder placed perpendicular to the main borehole in a particular azimuth and thus it will have much more limited area of fluid-formation interface. For this reason we call our model ”idealized (disk-shaped) perforation”. With all these limitations ”idealized perforation model” is a useful first step since it can be easily treated by cylindrically symmetric approaches at hand: effective wavenumber scheme and radially symmetric elastic finite-difference code. Material parameters are given in the Table 1 below. Obtained reflection coefficients are given on Figure 9 and Figure 10 for the case of finite-length (0.1 m) and zero-length perforations respectively. The latter one represents a case where there is only a break in the casing but radius of formation interface remains constant. In both cases the height of the perforation was 0.8 m. Again agreement is excellent between 1D approach and finite-difference numerical simulation. In case of a finite-length perforation (Figure 9) reflection is completely dominated by diameter change and is not dependent on casing parameters, whereas for zero-length perforation (Figure 10)

steel casing leads to slightly higher reflection.

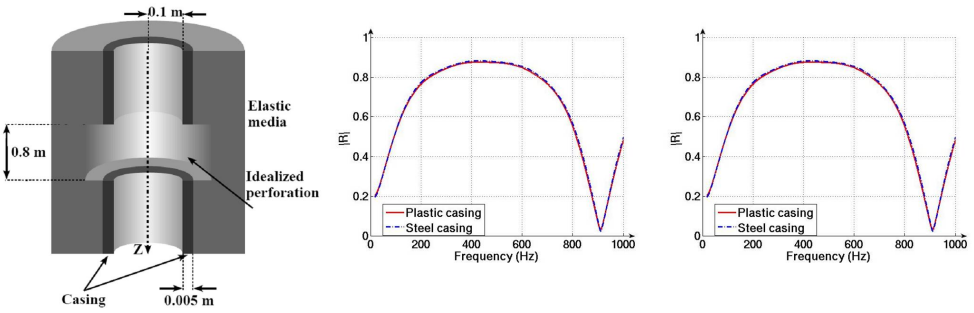


Fig. 8: Idealized model of a disk-shaped perforation (with no-flow at the sand face).

Fig. 9: Reflection of tube wave from perforation with 10 cm length for two cases: plastic casing (red line) and steel casing (blue line).

Fig. 10: Reflection of tube wave from zero-length perforation for two cases: plastic casing (red line) and steel casing (blue line). Solid lines - finite difference code; dashed lines - 1D effective wavenumber approach.

# 5 Limitations of 1D effective wavenumber approach

While previous publications (White, 1983; Tezuka et al, 1997) implied that 1D approach always works at low frequencies, we discovered that it can only be applied to models with ratio of layer thickness $h$ to borehole radius $R$ of more than two $(h > 2R)$. To understand the underlying reasons let us revert to the case of open borehole in homogeneous elastic formation. At low frequency tube-wave velocity is given by White (1983) as:

$$\frac{1}{c_t} = \sqrt{\rho\Big(\frac{1}{B} + \frac{1}{M}\Big)}, \tag{5.1}$$

where $\rho$ and $B$ are fluid density and bulk modulus, $M$ is formation shear modulus. If layers are introduced, then 1D approach assumes that velocity in each zone is still described by the same equation and is not distorted by layer boundaries. Since we can not verify this directly by velocity measurement in a thin layer, we perform an indirect quasi-static diagnostics. For infinite borehole surrounded with homogeneous formation the tube-wave velocity is deduced from this static elasticity relationship (White, 1983)

$$\frac{u_r}{R} - \frac{p}{2M} = 0 \tag{5.2}$$

on the boundary between fluid in the borehole and elastic formation. Here $u_r$ is radial displacement on the borehole wall, $p$ - fluid pressure, $R$ - borehole radius. If tube-wave velocity is to be described by equation (5.1) within each layer, then equation (5.2) should hold at each point of the fluid-formation boundary. However even for two elastic half-spaces instead of homogeneous media these conditions do not hold in a vicinity of a boundary between half-spaces. The absolute value of deviation from zero for the last expression (computed with finite-difference code) is presented on Figure 11.

The model under consideration is thin elastic layer $(0.6\ m < z < 1\ m)$ intersected with an open borehole $(R = 0.1\ m, h = 4R)$. Figure 11 shows that biggest deviations occur around the layer

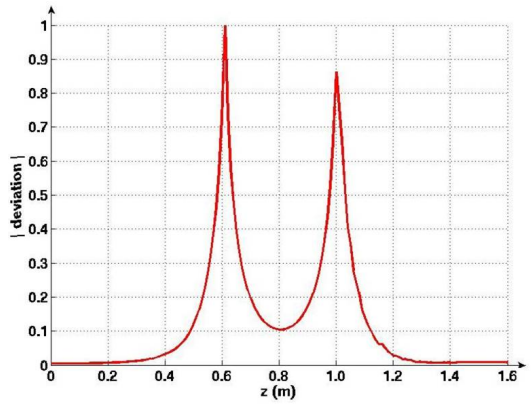


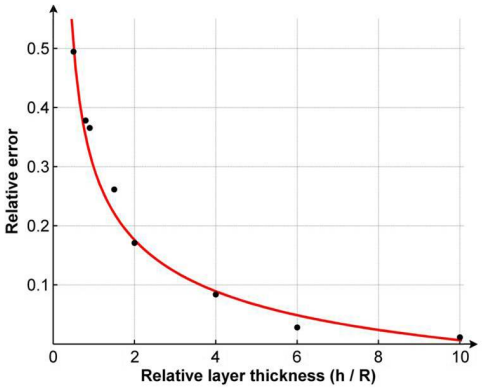


Fig. 11: Deviation $\left(\frac{|u_r/R - p/2M|}{\max|u_r/R - p/2M|}\right)$ from static formula (5.2) for a case of thin layer between two half-spaces.

Fig. 12: Relative error of 1D approach in respect to finite-difference modelling as a function of relative layer thickness

boundaries and two symmetric peaks overlap in the middle of the thin layer. Most likely mismatch of acoustic properties between fully bonded layers of different materials invalidate relation (5.2) near the interface. For two half-space model or this model with $h = 4R$ 1D this deviation is not essential and 1D approach still produces reflection response that is close to finite-difference computation. When layer thickness is further reduced, the deviation in the middle of the layer is enhanced by stronger interference of the approaching peaks. For thicknesses $h < 2R$ we observe consistent and substantial mismatches between the 1D approach and finite difference responses. It is clear that formula (5.2) is no longer valid within the layer and thus equation (5.1) does not represent a tube-wave velocity inside the bed with very close boundaries. We can interpret that that "effective" tube-wave velocity inside the thin layer is altered and is no longer described by (5.1), thus leading to a mismatch. Presence of multiple closely spaced geological interfaces between contrasting beds can break the approximations (5.2) and (5.1) in a larger depth interval. Therefore 1D wavenumber approach can not be applied to the case of very thin layers $(h < 2R)$.

# 6 Conclusions

We extended 1D effective wavenumber approach to treat the interactions of low-frequency tube waves with various borehole structures in a radially inhomogeneous media that supports single tube-wave mode. In particular, we have shown good agreement between responses obtained with 1D approach and finite-difference computations in cased boreholes with vertical variation in properties of casing or formation layers. We further tested this method for simplest model of idealized (disk-shaped) perforation with no-flow boundary at the sand face. In this case change in diameter is additionally introduced. We also demonstrate that 1D approach becomes inaccurate for very thin layers $(h < 2R)$ and thus very thin layers or small perforations can not be treated properly. We predict that in case of poroelastic structures 1D effective wavenumber approach would also account for fluid flow effects and correctly describe tube-wave interaction with radially inhomogeneous permeable formations.

# References


1. Bakulin A., Gurevich, B., Ciz, R., Ziatdinov S., 2005, Tube-wave reflection from a porous permeable layer with an idealized perforation: 75th Annual Meeting, Society of Exploration Geophysicists, Expanded Abstract, 332-335.

2. Krauklis, P. V., and A. P. Krauklis, 2005, Tube Wave Reflection and Transmission on the Fracture: 67th Meeting, EAGE, Expanded Abstracts, P217.

3. Medlin, W.L., Schmitt, D.P., 1994, Fracture diagnostics with tube-wave reflections logs: Journal of Petroleum Technology, March, 239-248.

4. Paige, R.W., L.R. Murray, and J.D.M. Roberts, 1995, Field applications of hydraulic impedance testing for fracture measurements: SPE Production and Facilities, February, 7-12.

5. Tang, X. M., and C. H. Cheng, 1993, Borehole Stoneley waves propagation across permeable structures: Geophysical Prospecting, 41, 165-187.

6. Tezuka, K., C.H. Cheng, and X.M. Tang, 1997, Modeling of low-frequency Stoneley-wave propagation in an irregular borehole: Geophysics, 62, 1047-1058.

7. White, J. E., 1983, Underground sound, Elsevier.

8. Winkler, K. W., H. Liu, and D.L. Johnson, 1989, Permeability and borehole Stoneley waves: Comparison between experiment and theory: Geophysics, 54, 66-75.

| | P-wave velocity (m/s) | S-wave velocity (m/s) | Density (kg/m$^3$) |
|---|---|---|---|
| Elastic half-spaces | 3500 | 2500 | 3400 |
| Casing 1 (steel) | 6000 | 3000 | 7000 |
| Casing 2 (plastic) | 2840 | 1480 | 1200 |
| Fluid | 1500 | - | 1000 |
| Layer 1 | 3100 | 1800 | 2600 |
| Layer 2 | 3700 | 2400 | 3000 |
| Corroded region 1 | 1200 | 600 | 1400 |
| Corroded region 2 | 3000 | 1500 | 3500 |
| Corroded region 3 | 4200 | 2100 | 4900 |

Table 1: material parameters